

## Local density of states and Friedel oscillations in graphene

Ádám Bácsi<sup>1,\*</sup> and Attila Virosztek<sup>1,2,†</sup>

<sup>1</sup>*Department of Physics, Budapest University of Technology and Economics, 1521 Budapest, Hungary*

<sup>2</sup>*Research Institute for Solid State Physics and Optics, P.O. Box 49, 1525 Budapest, Hungary*

(Received 16 September 2010; published 11 November 2010)

We investigate the local density of states and Friedel oscillation in graphene around a well-localized impurity in Born approximation. In our analytical calculations Green's function technique has been used taking into account both the localized atomic wave functions in a tight-binding scheme and the corresponding symmetries of the lattice. As a result we obtained long wavelength oscillations in the density of electrons with long-range behavior proportional to the inverse square of the distance from the impurity. These leading oscillations are out of phase on nearby lattice sites (in fact for an extended defect they cancel each other within one unit cell), therefore a probe with resolution worse than a few unit cells will experience only the next to leading inverse cube decay of density oscillations even for a short-range scatterer.

DOI: [10.1103/PhysRevB.82.193405](https://doi.org/10.1103/PhysRevB.82.193405)

PACS number(s): 81.05.ue, 73.22.Pr, 73.22.Dj, 74.55.+v

Ever since the first production of atomically thin carbon films,<sup>1</sup> graphene continues to fascinate physicists of almost all walks of life. This simple two-dimensional system of carbon atoms arranged in a honeycomb lattice provides us with a number of interesting properties mainly due to the massless Dirac nature of the dispersion relation of its electrons.<sup>2</sup> Undoped graphene has its Fermi energy at the tip of the Dirac cones and behaves as a zero-gap semiconductor. Applying appropriate gate voltage leads to electron or hole pockets and metallic behavior with Fermi wave number  $k_F$  typically much smaller than the size of the Brillouin zone. Exciting potential applications of graphene include for example carbon-based planar electronic circuitry with the possibility of electrically reconfigurable wiring,<sup>3</sup> exploiting the guiding effect of graphene  $p$ - $n$  junctions with negative refractive index.<sup>4</sup> On the theoretical side perhaps the simplest quantity to be considered is the change in the local density of states (LDOS) and the Friedel oscillation (FO) in the excess charge density due to a well-localized impurity. Results of these considerations have implications for the LDOS in disordered graphene,<sup>5,6</sup> for the interaction between adatoms in graphene,<sup>7,8</sup> or in case of magnetic adatoms<sup>9</sup> for the corresponding Ruderman-Kittel-Kasuya-Yosida (RKKY) interaction.<sup>10</sup>

Early theoretical work on the LDOS and the resulting FO around an impurity in graphene<sup>11,12</sup> predicted long-wavelength ( $2k_F$ ) oscillations in the charge density, but with envelope decaying like  $r^{-3}$  at distance  $r$  from the impurity. This is in contrast to the  $r^{-2}$  decay in a degenerate nonrelativistic two-dimensional Fermi gas, and suppressed back-scattering of chiral graphene electrons residing around the Fermi circle of the Dirac cone was offered as an explanation. However, graphene has two inequivalent Dirac cones (valleys) in the Brillouin zone and intervalley scattering by the impurity may lead to short wavelength oscillations on the order of a few lattice constants as well. Indeed, a scanning tunneling microscopy (STM) study<sup>13</sup> of epitaxial graphene revealed two different length scales around defects. Subsequently, intervalley (or internodal) scattering has been built in the theory<sup>14</sup> and has been shown to be responsible for  $r^{-1}$  decay in LDOS and  $r^{-2}$  decay in FO. The different power laws for intranodal and internodal scatterings have been ob-

served by Fourier Transform STM experiment<sup>15</sup> but no detailed investigation of the short-wavelength oscillations has been performed either experimentally or theoretically. The first step toward this direction has been made by incorporating atomic wave functions instead of just plane waves into the theory,<sup>16</sup> and it has become clear that although the LDOS falls off with  $r^{-1}$ , for intranodal scattering only it has opposite sign on the two sublattices. Therefore upon coarse graining, for example, due to experimental resolution, the leading order decay cancels within one unit cell, and one is left with the next to leading  $r^{-2}$  envelope, and consequently an  $r^{-3}$  decay of FO.

The aim of the present Brief Report is to give a detailed analysis of the short wavelength oscillations due to internodal scattering within the framework of a simple and transparent, atomic resolution theory based on the tight-binding wave functions of electrons on the honeycomb lattice. Our main results are the short-range spatial pattern of LDOS and FO on both sublattices with the corresponding symmetries (see Fig. 1), and the observation that including internodal scattering still lead to cancellation of the leading power law decay of oscillations, but not within one unit cell, but within three neighboring ones. This means that if, for example, the STM tip cannot resolve the six atoms on a hexagon of the honeycomb lattice, we encounter again just the next to leading power law envelopes for both LDOS and FO.

We begin with the tight-binding Hamiltonian of carbon atoms forming a honeycomb lattice with nearest-neighbor hopping  $t$  (assumed to be real) between the  $p_z$  orbitals  $\varphi(\mathbf{r})$ . In momentum space this leads to a  $2 \times 2$  Hamiltonian matrix spanned by Bloch waves constructed from the atomic orbitals on the two sublattices  $A$  and  $B$  as

$$H = \sum_{\mathbf{k}\sigma} \begin{pmatrix} a_{A\mathbf{k}\sigma}^+ & a_{B\mathbf{k}\sigma}^+ \end{pmatrix} \begin{pmatrix} 0 & tf^*(\mathbf{k}) \\ tf(\mathbf{k}) & 0 \end{pmatrix} \begin{pmatrix} a_{A\mathbf{k}\sigma} \\ a_{B\mathbf{k}\sigma} \end{pmatrix}, \quad (1)$$

where  $f(\mathbf{k}) = 1 + e^{ika_1} + e^{ika_2}$  with primitive lattice vectors  $\mathbf{a}_{1,2} = a(\pm 1/2, \sqrt{3}/2)$  of length  $a$ . Diagonalization yields the eigenvalues  $\varepsilon_{\pm}(\mathbf{k}) = \pm |t| |f(\mathbf{k})|$  defining the two bands of pure graphene and the eigenvectors in the tight-binding form

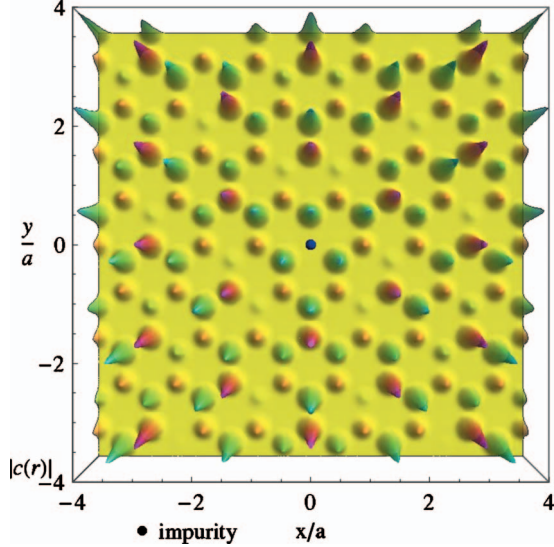


FIG. 1. (Color) Short-wavelength spatial dependence of the LDOS due to an impurity at the center. Three-dimensional plot of  $c_A(\mathbf{r})+c_B(\mathbf{r})=|c(\mathbf{r})|$  is viewed from above and the color code indicates the opposite sign on the two sublattices.

$$\Psi_{\pm,\mathbf{k}}(\mathbf{r}) = \frac{1}{\sqrt{N}} \sum_{\mathbf{R}} e^{i\mathbf{k}\mathbf{R}} [\mp e^{-i\delta(\mathbf{k})} \varphi(\mathbf{r}-\mathbf{R}) + \varphi(\mathbf{r}-\mathbf{R}-\mathbf{c})], \quad (2)$$

where the summation runs over the  $\mathbf{R}$  lattice vectors and  $\delta(\mathbf{k})$  is the complex phase of  $f(\mathbf{k})$  determining the mixing of  $A$  and  $B$  sublattice states, and  $\mathbf{c}=(\mathbf{a}_1+\mathbf{a}_2)/3$  is the vector pointing from the  $A$  to the  $B$  site within the unit cell. As is well known,  $f(\mathbf{k})$  vanishes at the corners of the hexagonal Brillouin zone, leading to the massless Dirac spectrum  $\varepsilon_{\pm}(\mathbf{k}) \approx \pm \hbar v_F \delta k$ , with  $v_F = \sqrt{3}a|t|/2\hbar$  the Fermi velocity, and  $\delta k$  the wave number measured from the corners. Since there are two inequivalent corners, for example,  $\mathbf{K}=(\mathbf{b}_1-\mathbf{b}_2)/3$  and  $\mathbf{K}'=-\mathbf{K}$  as expressed by the primitive reciprocal lattice vectors, there are two Dirac cones or valleys in the Brillouin zone. Electron spin does not play any role in the forthcoming discussion, therefore we suppress spin indices, and all our results will refer to one spin orientation.

The real-space representation of the Green's function of complex energy variable  $G(z, \mathbf{r}, \mathbf{r}')$  is of central importance for our subject since the LDOS is given by its analytic continuation just above the real axis as  $\rho(\varepsilon, \mathbf{r}) = -\pi^{-1} \text{Im} G(\varepsilon + i\delta, \mathbf{r}, \mathbf{r})$ . For pure graphene, not perturbed by impurities, the free Green's function is evaluated using Eq. (2) as

$$G^0(z, \mathbf{r}, \mathbf{r}') = \sum_{l=\pm, \mathbf{k}} \frac{\Psi_{l,\mathbf{k}}(\mathbf{r}) \Psi_{l,\mathbf{k}}^*(\mathbf{r}')}{z - \varepsilon_l(\mathbf{k})} = \sum_{\mathbf{R}, \mathbf{R}'} \varphi(\mathbf{r}-\mathbf{R}) \mathbf{G}^0(z, \mathbf{R}-\mathbf{R}') \varphi^+(\mathbf{r}'-\mathbf{R}'), \quad (3)$$

where  $\varphi(\mathbf{r}) = [\varphi(\mathbf{r}), \varphi(\mathbf{r}-\mathbf{c})]$  is a row vector formed by the

orbitals of the  $A$  and  $B$  sites in the unit cell, and the Green's matrix is given by

$$\mathbf{G}^0(z, \mathbf{R}) = \frac{1}{N} \sum_{\mathbf{k}} \frac{e^{i\mathbf{k}\mathbf{R}}}{z^2 - t^2 |f(\mathbf{k})|^2} \begin{pmatrix} z & tf^*(\mathbf{k}) \\ tf(\mathbf{k}) & z \end{pmatrix}. \quad (4)$$

The free Green's function in Eq. (3) is clearly translation invariant by a lattice vector only but due to the well-localized nature of the atomic wave functions it typically consists of only one non-negligible term determined by the proximity of  $\mathbf{r}$  and  $\mathbf{r}'$  to a lattice point given by either  $\mathbf{r}_A(=\mathbf{R})$  on the  $A$  sublattice or by  $\mathbf{r}_B(=\mathbf{R}+\mathbf{c})$  on the  $B$  sublattice. On the other hand, the (identical) diagonal elements of the Green's matrix in Eq. (4) are even functions of  $\mathbf{R}$  [e.g.,  $G_{AA}^0(z, -\mathbf{R}) = G_{AA}^0(z, \mathbf{R})$ ] while the off-diagonal elements transform into each other upon reflection [ $G_{AB}^0(z, -\mathbf{R}) = G_{BA}^0(z, \mathbf{R})$ ]. It is instructive to consider the LDOS of the pure system given by  $\rho_0(\varepsilon, \mathbf{r}) = \rho_0(\varepsilon) \sum_{\mathbf{R}} [|\varphi(\mathbf{r}-\mathbf{R})|^2 + |\varphi(\mathbf{r}-\mathbf{R}-\mathbf{c})|^2]/2$ , where  $\rho_0(\varepsilon)$  is the DOS, which can be approximated around the Dirac point by  $A_c |\varepsilon| / \pi (\hbar v_F)^2$ ,  $A_c = \sqrt{3}a^2/2$  being the area of the unit cell.

Let us consider a substitutional impurity characterized by a short-range scattering potential energy  $U(\mathbf{r}) = u\delta(\mathbf{r})$  located at the origin, which is a site on the  $A$  sublattice. The correction to the LDOS in Born approximation is determined by  $\Delta G(z, \mathbf{r}, \mathbf{r}) = uG^0(z, \mathbf{r}, 0)G^0(z, 0, \mathbf{r})$ , which can be expressed due to the localized atomic orbitals as

$$u_0 |\varphi(\mathbf{r}-\mathbf{r}_A)|^2 G_{AA}^0(z, \mathbf{r}_A) G_{AA}^0(z, -\mathbf{r}_A) \quad (5)$$

or

$$u_0 |\varphi(\mathbf{r}-\mathbf{r}_B)|^2 G_{BA}^0(z, \mathbf{r}_B-\mathbf{c}) G_{AB}^0(z, -\mathbf{r}_B+\mathbf{c}) \quad (6)$$

depending on whether  $\mathbf{r}$  is in the vicinity of an  $A$  or a  $B$  site, respectively, and  $u_0 = u|\varphi(0)|^2$ . Corrections to the LDOS beyond Born approximation are negligible as long as  $u_0 \rho_0(\varepsilon) \ll 1$ , or  $u_0 \ll t^2/|\varepsilon|$ . Considering higher order terms within say a  $T$ -matrix approximation would lead primarily to bound states localized around the impurity,<sup>17</sup> the description of which is out of scope of the present Brief Report. The spatial pattern in Eqs. (5) and (6) is dominated by the density profile of the atomic orbital centered on the given lattice site while the multiplicative factor on that site depends on the corresponding Green's matrix elements. It can be proven that the diagonal elements of the Green's matrix such as  $G_{AA}^0(z, \mathbf{r}_A)$  have sixfold rotational symmetry in  $\mathbf{r}_A$ , while the off-diagonal elements such as  $G_{BA}^0(z, \mathbf{r}_B-\mathbf{c})$  have only threefold rotational symmetry in  $\mathbf{r}_B$ .

In order to evaluate the relevant Green's matrix elements from Eq. (4) we observe that the most important contributions come from the nodal points of the spectrum, i.e., from around the points  $\mathbf{K}$  and  $\mathbf{K}'=-\mathbf{K}$  in the Brillouin zone. The matrix elements therefore consist of two terms each, led by fast oscillations of the type  $\exp(i\mathbf{K}\mathbf{R})$  and  $\exp(i\mathbf{K}'\mathbf{R})$ , modulated by functions of slow spatial variation. These latter functions can be evaluated by using the linearized  $f(\pm\mathbf{K}+\delta\mathbf{k}) = -\sqrt{3}a(\pm\delta k_x + i\delta k_y)/2$  expression around the nodal points up to a cutoff  $k_c$ . This will be a good approximation for these slowly varying factors of the Green's matrix

elements for distances from the impurity much larger and for characteristic spatial variations much longer than  $1/k_c$ . This procedure leads to the following result for the diagonal element in Eq. (5):

$$G_{AA}^0(z, \mathbf{r}_A) = (e^{i\mathbf{K}\mathbf{r}_A} + e^{i\mathbf{K}'\mathbf{r}_A}) \frac{-iA_c z}{(2\hbar v_F)^2} H_0^{(1)}\left(\frac{zr_A}{\hbar v_F}\right), \quad (7)$$

where  $H_0^{(1)}(z)$  is the Hankel function, and this functional form is valid for  $\text{Im } z > 0$  only (which is enough for the prescribed analytic continuation) and for  $|z| \ll \hbar v_F k_c$ . Similarly, for the off-diagonal element in Eq. (6) we obtain

$$G_{BA}^0(z, \mathbf{r}_B - \mathbf{c}) = (e^{i(\mathbf{K}\mathbf{r}_B + \vartheta)} - e^{i(\mathbf{K}'\mathbf{r}_B - \vartheta)}) \times \frac{-\text{sgn}(t)A_c z}{(2\hbar v_F)^2} H_1^{(1)}\left(\frac{zr_B}{\hbar v_F}\right), \quad (8)$$

where  $H_1^{(1)}(z) = -dH_0^{(1)}(z)/dz$ ,  $\vartheta$  is the angle  $\mathbf{r}_B$  makes with the  $x$  axis (which is parallel to  $\mathbf{K}$ ). For  $G_{AB}^0(z, -\mathbf{r}_B + \mathbf{c})$  we have the same formula as in Eq. (8), except that the prefactor with the exponentials is replaced by  $(-e^{-i(\mathbf{K}\mathbf{r}_B + \vartheta)} + e^{-i(\mathbf{K}'\mathbf{r}_B - \vartheta)})$ . We remind the reader that these exponential prefactors in the Green's matrix elements describing short-wavelength oscillations are exact, as opposed to the spatial dependence described by the Hankel functions.

The change in the LDOS in graphene due to the impurity  $\Delta\rho(\varepsilon, \mathbf{r}) = -\pi^{-1} \text{Im } \Delta G(\varepsilon + i\delta, \mathbf{r}, \mathbf{r})$  is now easily calculated using Eqs. (5)–(8). Let us note first, that the short-wavelength spatial pattern in, e.g., Eq. (5) is given as  $(e^{i\mathbf{K}\mathbf{r}_A} + e^{i\mathbf{K}'\mathbf{r}_A})(e^{-i\mathbf{K}\mathbf{r}_A} + e^{-i\mathbf{K}'\mathbf{r}_A}) = 4 \cos^2(\mathbf{K}\mathbf{r}_A)$ . However, if the impurity is unable to produce intervalley scattering (e.g., because it is extended and has no large wave-number Fourier components), then plane waves belonging to different valleys will not contribute to the above product, and we will only have  $1+1=2$  as a result. Thus, without intervalley scattering, the factor  $\cos^2(\mathbf{K}\mathbf{r}_A)$  describing the short-wavelength spatial pattern should be replaced by its average, i.e.,  $1/2$ . The same is true for the factor  $\sin^2(\mathbf{K}\mathbf{r}_B + \vartheta)$  appearing in Eq. (6).

Returning to the change in the LDOS, after analytic continuation we obtain

$$\Delta\rho(\varepsilon, \mathbf{r}) = \frac{\pi}{2} u_0 c_A(\mathbf{r}) \rho_0^2(\varepsilon) \text{sgn}(\varepsilon) J_0\left(\frac{|\varepsilon|r_A}{\hbar v_F}\right) Y_0\left(\frac{|\varepsilon|r_A}{\hbar v_F}\right) \quad (9)$$

if  $\mathbf{r}$  is in the vicinity of an  $A$  site and

$$\Delta\rho(\varepsilon, \mathbf{r}) = \frac{\pi}{2} u_0 c_B(\mathbf{r}) \rho_0^2(\varepsilon) \text{sgn}(\varepsilon) J_1\left(\frac{|\varepsilon|r_B}{\hbar v_F}\right) Y_1\left(\frac{|\varepsilon|r_B}{\hbar v_F}\right) \quad (10)$$

if  $\mathbf{r}$  is in the vicinity of a  $B$  site. Here  $J_0$ ,  $J_1$  and  $Y_0$ ,  $Y_1$  are Bessel functions of the first and the second kind. The factors describing the short-wavelength spatial behavior are given by

$$c_A(\mathbf{r}) = |\varphi(\mathbf{r} - \mathbf{r}_A)|^2 \cos^2(\mathbf{K}\mathbf{r}_A) \quad (11)$$

and

$$c_B(\mathbf{r}) = |\varphi(\mathbf{r} - \mathbf{r}_B)|^2 \sin^2(\mathbf{K}\mathbf{r}_B + \vartheta). \quad (12)$$

It can be easily proven that the  $c_A(\mathbf{r})$  and  $c_B(\mathbf{r})$  factors are invariant under sixfold and threefold rotations, respectively. Let us remember that for intravalley scattering only, the weights of the density of atomic orbitals would be the same on each atoms. We note here that the relative change in the LDOS not too far from the impurity is  $\Delta\rho(\varepsilon, \mathbf{r})/\rho_0(\varepsilon, \mathbf{r}) \approx u_0 \rho_0(\varepsilon)$ , therefore within the region of applicability of the Born approximation, in order to observe  $\Delta\rho(\varepsilon, \mathbf{r})$  by STM, an intensity resolution is required which is comparable to or better than what is needed for observing  $\rho_0(\varepsilon, \mathbf{r})$ .

The isotropic spatial dependence in the LDOS given by the Bessel functions in Eqs. (9) and (10) describes long-wavelength oscillations since the characteristic wave number  $k = \varepsilon/\hbar v_F$  is much smaller than the cutoff  $k_c$ . Consequently, instead of  $r_A$  and  $r_B$  we can use here the continuous variable  $r$  measuring the distance from the impurity. For distances large enough to satisfy  $|k|r \gg 1$  we can use the leading asymptotic expressions  $J_1(x)Y_1(x) = \cos(2x)/\pi x = -J_0(x)Y_0(x)$  for  $x \rightarrow \infty$ . Due to this sign change on the two sublattices, it is useful to define a composite short-wavelength pattern  $c(\mathbf{r}) = -c_A(\mathbf{r})$  if  $\mathbf{r}$  is near an  $A$  site, and  $c(\mathbf{r}) = c_B(\mathbf{r})$  if  $\mathbf{r}$  is near a  $B$  site. Then the change in the LDOS due to an impurity at the origin can be given by the following compact formula:

$$\Delta\rho(\varepsilon, \mathbf{r}) = u_0 c(\mathbf{r}) \rho_0^2(\varepsilon) \frac{\cos(2kr)}{2kr} \quad (13)$$

indicating a long-wavelength oscillation with an  $r^{-1}$  decay and a short wavelength spatial pattern given by  $c(\mathbf{r})$ , and shown in Fig. 1. Although a very rich structure can be seen on the plot, the overall threefold rotational symmetry is apparent, and appears to have been observed experimentally.<sup>18</sup>

Due to finite resolution however, the STM tip will measure a spatial average of the pattern on Fig. 1. In the simpler case of an extended impurity not producing intervalley scattering,  $c(\mathbf{r})$  has atomic densities with equal weight on each site of one sublattice and the same weight with opposite sign on each site of the other sublattice. Clearly, a resolution worse than an elementary cell of graphene will lead to cancellation of the leading  $r^{-1}$  decay in Eq. (13), leaving us with the next to leading  $r^{-2}$  decay of LDOS. On the other hand for a short range impurity potential, internodal scattering contributes as well, and yields the short wavelength spatial pattern on Fig. 1, where no cancellation within one unit cell occurs. However it is easily shown, that averaging  $c(\mathbf{r})$  over three neighboring unit cells again leads to cancellation of the weights of the atomic densities. Indeed if the weights in  $c(\mathbf{r})$  are added in the unit cells given by lattice vectors  $\mathbf{R}$ ,  $\mathbf{R} + \mathbf{a}_1$ , and  $\mathbf{R} + \mathbf{a}_1 - \mathbf{a}_2$  (far from the impurity  $\vartheta$  is the same for all three lattice sites), we obtain zero. Therefore an STM with resolution worse than three elementary cells will not be able to measure the leading  $r^{-1}$  decay either. It is easily shown that the weights of the atomic densities cancel on the six sites of any hexagon of the honeycomb lattice.

The change in the particle density at zero temperature due to the impurity is now easily obtained by integrating the LDOS up to the Fermi energy  $\varepsilon_F$ . Since  $\Delta\rho(\varepsilon, \mathbf{r})$  is an odd

function of energy,  $\Delta n(\mathbf{r})$  is even in  $\varepsilon_F$ , therefore we integrate up to  $-\varepsilon_F$ . As long as  $k_F r \gg 1$ , where  $k_F = |\varepsilon_F|/\hbar v_F$ , we can use the asymptotic forms of the Bessel functions to obtain the leading term of the FO as

$$\Delta n(\mathbf{r}) = \frac{u_0 A_c}{4\pi} c(\mathbf{r}) \rho_0(\varepsilon_F) \frac{\sin(2k_F r)}{r^2}, \quad (14)$$

where we disregarded the oscillations due to the cutoff at the lower limit of integration as unphysical since these are too fast to be taken seriously in our scheme. The FO with wave number  $2k_F$  decays on both sublattice as  $r^{-2}$ , but as it was discussed in case of the LDOS, limited experimental resolution leads to cancellation of the leading power laws, and only the  $r^{-3}$  decay will be observed. For resolution of about a unit cell this happens for an extended impurity not producing internodal scattering, but somewhat worse resolution of about three unit cells or a hexagon of the honeycomb lattice leads to cancellation even for a pointlike impurity producing internodal scattering as well. Finally it is worth mentioning that for half-filled graphene, i.e.,  $\varepsilon_F=0$ , we obtain  $r^{-3}$  decay without  $2k_F$  oscillations on both sublattices.

In conclusion, we have presented a clear and concise calculation of the change in the local density of states, and the resulting Friedel oscillations in the electron density in graphene, due to a single nonmagnetic substitutional impurity with short-range scattering potential. In order to achieve atomic scale description we used tight-binding wave functions with atomic orbitals. As a consequence of this approach, the short wavelength spatial pattern in our results for both LDOS and FO, described by  $c(\mathbf{r})$  in Eqs. (13) and (14),

can be considered exact. Using a linearized electronic spectrum up to a cutoff affects only the rest of the spatial dependence but for energies close to the Dirac point and for distances far from the impurity, the long-wavelength oscillating parts are excellent approximations as well. In particular, the LDOS decays as  $r^{-1}$  and the FO with wave number  $2k_F$  as  $r^{-2}$  on both sublattices. The short-wavelength spatial pattern, depicted on Fig. 1, shows the required rotational symmetries. Since  $c(\mathbf{r})$  has alternating signs on neighboring lattice sites, experimental resolution worse than about three unit cells (or a hexagon of the lattice) will lead to cancellation of the leading power-law decays in both quantities yielding the next to leading  $r^{-2}$  and  $r^{-3}$  behaviors for LDOS and FO, respectively. Within the present framework, the case of an extended defect can also be considered by restricting the calculation to intravalley scattering by the impurity. This affects only the short wavelength spatial pattern  $c(\mathbf{r})$ , making the weights of the atomic densities in it equal (but still of opposite sign on the two sublattices). Consequently, the above mentioned cancellation of the leading power-law decays occurs already at resolution worse than one unit cell. Therefore if the experimental resolution falls between one and three unit cells, distinction can be made between localized and extended defects, since the observed power-law decay for LDOS, for example, should follow  $r^{-1}$  for the former and  $r^{-2}$  for the latter.

We have benefited from discussions with B. Dóra and J. Cserti. This work was supported by the Hungarian Scientific Research Fund under Grants No. OTKA K72613 and No. TÁMOP-4.2.1/B-09/1/KMR-2010-0002.

\*bacs.adam@wigner.bme.hu

†viro@szfki.hu

<sup>1</sup>K. S. Novoselov, A. K. Geim, S. V. Morozov, D. Jiang, Y. Zhang, S. V. Dubonos, I. V. Grigorieva, and A. A. Firsov, *Science* **306**, 666 (2004).

<sup>2</sup>A. H. Castro Neto, F. Guinea, N. M. R. Peres, K. S. Novoselov, and A. K. Geim, *Rev. Mod. Phys.* **81**, 109 (2009).

<sup>3</sup>J. Williams, T. Low, M. Lundstrom, and C. Marcus, [arXiv:1008.3704](https://arxiv.org/abs/1008.3704) (unpublished).

<sup>4</sup>J. Cserti, A. Pályi, and C. Péterfalvi, *Phys. Rev. Lett.* **99**, 246801 (2007).

<sup>5</sup>K. Ziegler, B. Dóra, and P. Thalmeier, *Phys. Rev. B* **79**, 235431 (2009).

<sup>6</sup>N. M. R. Peres, L. Yang, and S. W. Tsai, *New J. Phys.* **11**, 095007 (2009).

<sup>7</sup>A. V. Shytov, D. A. Abanin, and L. S. Levitov, *Phys. Rev. Lett.* **103**, 016806 (2009).

<sup>8</sup>V. V. Cheianov, O. Syljuåsen, B. L. Altshuler, and V. I. Falko,

*Phys. Rev. B* **80**, 233409 (2009).

<sup>9</sup>B. Uchoa, L. Yang, S. W. Tsai, N. M. R. Peres, and A. H. Castro Neto, *Phys. Rev. Lett.* **103**, 206804 (2009).

<sup>10</sup>S. Saremi, *Phys. Rev. B* **76**, 184430 (2007).

<sup>11</sup>V. V. Cheianov and V. I. Falko, *Phys. Rev. Lett.* **97**, 226801 (2006).

<sup>12</sup>V. V. Cheianov, *Eur. Phys. J. Spec. Top.* **148**, 55 (2007).

<sup>13</sup>G. M. Rutter, J. N. Crain, N. P. Guisinger, T. Li, P. N. First, and J. A. Stroscio, *Science* **317**, 219 (2007).

<sup>14</sup>C. Bena, *Phys. Rev. Lett.* **100**, 076601 (2008).

<sup>15</sup>I. Brihuega, P. Mallet, C. Bena, S. Bose, C. Michaelis, L. Vitali, F. Varchon, L. Magaud, K. Kern, and J. Y. Veuillen, *Phys. Rev. Lett.* **101**, 206802 (2008).

<sup>16</sup>C. Bena, *Phys. Rev. B* **79**, 125427 (2009).

<sup>17</sup>M. M. Ugeda, I. Brihuega, F. Guinea, and J. M. Gómez-Rodríguez, *Phys. Rev. Lett.* **104**, 096804 (2010).

<sup>18</sup>L. Simon, C. Bena, F. Vonau, D. Aubel, H. Nasrallah, M. Habar, and J. C. Peruchetti, *Eur. Phys. J. B* **69**, 351 (2009).